Check for updates

Chemistry
Europe

European Chemical
Societies Publishing

VIP *Very Important Paper*

Special Collection

π-Extended Helical Nanographenes: Synthesis and Photophysical Properties of Naphtho[1,2-*a*]pyrenes**

Wesley A. Chalifoux,*[a] Paban Sitaula,[a] Ryan J. Malone,[a] Giovanna Longhi,[b]
Sergio Abbate,[b] Eva Gualtieri,[c] Andrea Lucotti,[c] Matteo Tommasini,[c] Roberta Franzini,[d]
Claudio Villani,[d] and Vincent J. Catalano[a]

A mild and efficient synthesis of a broad scope of substituted naphtho[1,2-*a*]pyrene derivatives was accomplished in good yields using an InCl$_3$/AgNTf$_2$-mediated two-fold alkyne benzannulation reaction. HPLC enantiomeric separation was achieved and the interconversion barriers have been determined. The ECD spectra of two derivatives were recorded and interpreted through TD-DFT calculations. Raman spectra were also recorded and predicted through DFT calculations.

Introduction

Nanographenes are substructures of graphene and have gained significant interest in the physical sciences because of the synthetic challenges they pose as well as their interesting structure-property relationships.[1] There is a lot of recent interest in using nanographenes in various optical and electronic devices.[2] Helicenes are an important class of nanographene having *ortho*-fused benzene rings that results in fascinating structures that make them useful in a variety of applications.[3] Incorporation of pyrene substructures into helicenes not only results in lateral extension of the π-system but also leads to unique structural and photophysical properties.[4] Naphtho[1,2-*a*]pyrenes are examples of small nanographene structures that derive from laterally π-extended [4]helicenes. There are limited synthetic methods for the synthesis of these pyrene-helicene hybrids. Desai and co-workers demonstrated that a Brønsted acid-catalyzed alkene-benzannulation reaction could be used for the synthesis of naphtho[1,2-*a*]pyrene (Figure 1a).[5] In 2020, Alabugin and coworkers synthesized naphtho[1,2-*a*]pyrenes using an elegant three-point double annulation via a radical cascade reaction (Figure 1b).[6] This methodology was extended to other facinating nanographenes such as naphtho[3,4-*a*]pyrenes, pyreno[1,2-*a*]pyrenes, and peropyrenes. Methods that incorporate substituents into the *cove* region of the [4]helicene core have also been achieved. For example, Collins and co-workers reported the synthesis of an electron-rich *cove*-substituted naphtho[1,2-*a*]pyrene using a photoredox flow-chemistry approach (Figure 1c).[7] The same methodology was applicable to the synthesis of π-extended [5]helicenes. Our group has been interested in harnessing the potential of high-energy alkyne-containing compounds in multi-fold benzannulation reactions to arrive at various achiral[8] and chiral nanographenes,[8a,c,9] as well as soluble graphene nanoribbons.[10] For example, we recently reported a Brønsted acid-catalyzed four-fold alkyne benzannulation reaction to fuse a second naphthyl group onto a naphtho[1,2-*a*]pyrene core and included two aryl groups within the *cove* to arrive at chiral pyreno[*a*]pyrene-based helicene hybrids (Figure 1d).[11] We have found that switching from Brønsted acids to Lewis acids allows us to synthesize a broader scope of substituted nanographenes.[8a,c] Here, we report the use of Lewis acid catalysis for the synthesis of broadly functionalized naphtho[1,2-*a*]pyrenes (Figure 1e). The reaction features a double alkyne benzannulation reaction that results in an aryl substituent within a newly formed *cove* region of a [4]helicene. We envisioned that this design feature would increase the inversion barrier of the [4]helicene core and allow for enantiomeric separation for spectroscopic studies. A version of this manuscript was submitted as a preprint.[12]

Results and Discussion

Synthesis

Our strategy for the synthesis of naphtho[1,2-*a*]pyrenes **1** starts with a Suzuki cross-coupling reaction between boronic esters **2**[8a,c,d] and 3-bromophenanthrenes **3**[13] to afford our key diyne intermediate **4**. The diyne was then subjected to a two-fold InCl$_3$/AgNTf$_2$-catalyzed alkyne benzannulation reaction[8a,c] to produce

[a] Prof. W. A. Chalifoux, Dr. P. Sitaula, R. J. Malone, Prof. V. J. Catalano
Department of Chemistry
University of Nevada, Reno
1664 North Virginia Street, Reno, Nevada 89557, United States
E-mail: wchalifoux@unr.edu
https://www.unr.edu/chemistry/faculty/wesley-chalifoux

[b] Dr. G. Longhi, Prof. S. Abbate
Departimento di Medicina Molecolare e Traslazionale
Università di Brescia
Viale Europa 11, 25123 Brescia, Italy

[c] E. Gualtieri, Dr. A. Lucotti, Prof. M. Tommasini
Dipartimento di Chimica, Materiali e Ingegneria Chimica "G. Natta"
Politecnico di Milano
Piazza Leonardo da Vinci 32, 20133, Milano, Italy

[d] R. Franzini, Prof. C. Villani
Dipartimento di Chimica e Tecnologie del Farmaco
Universitá di Roma "La Sapienza"
00185 Roma, Italy

EurJOC
European Journal of Organic Chemistry

Research Article
doi.org/10.1002/ejoc.202101466

**Chemistry
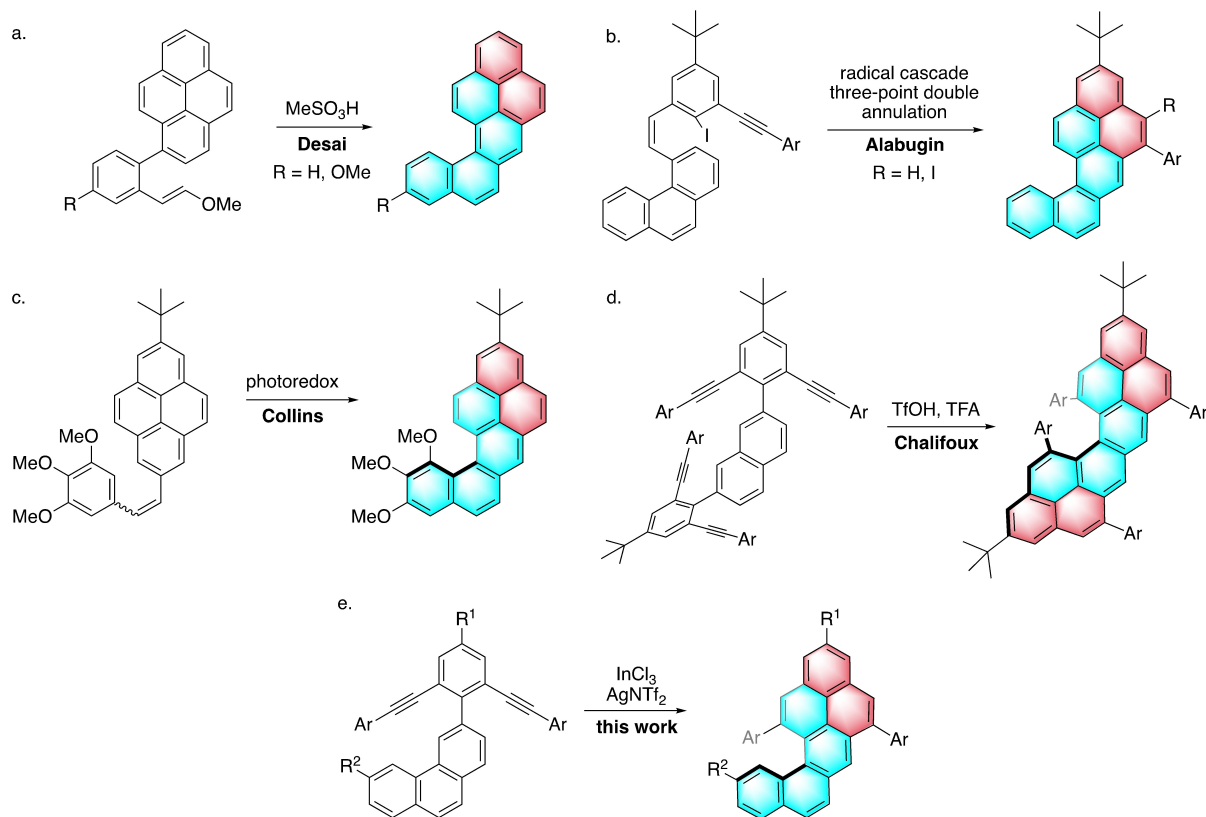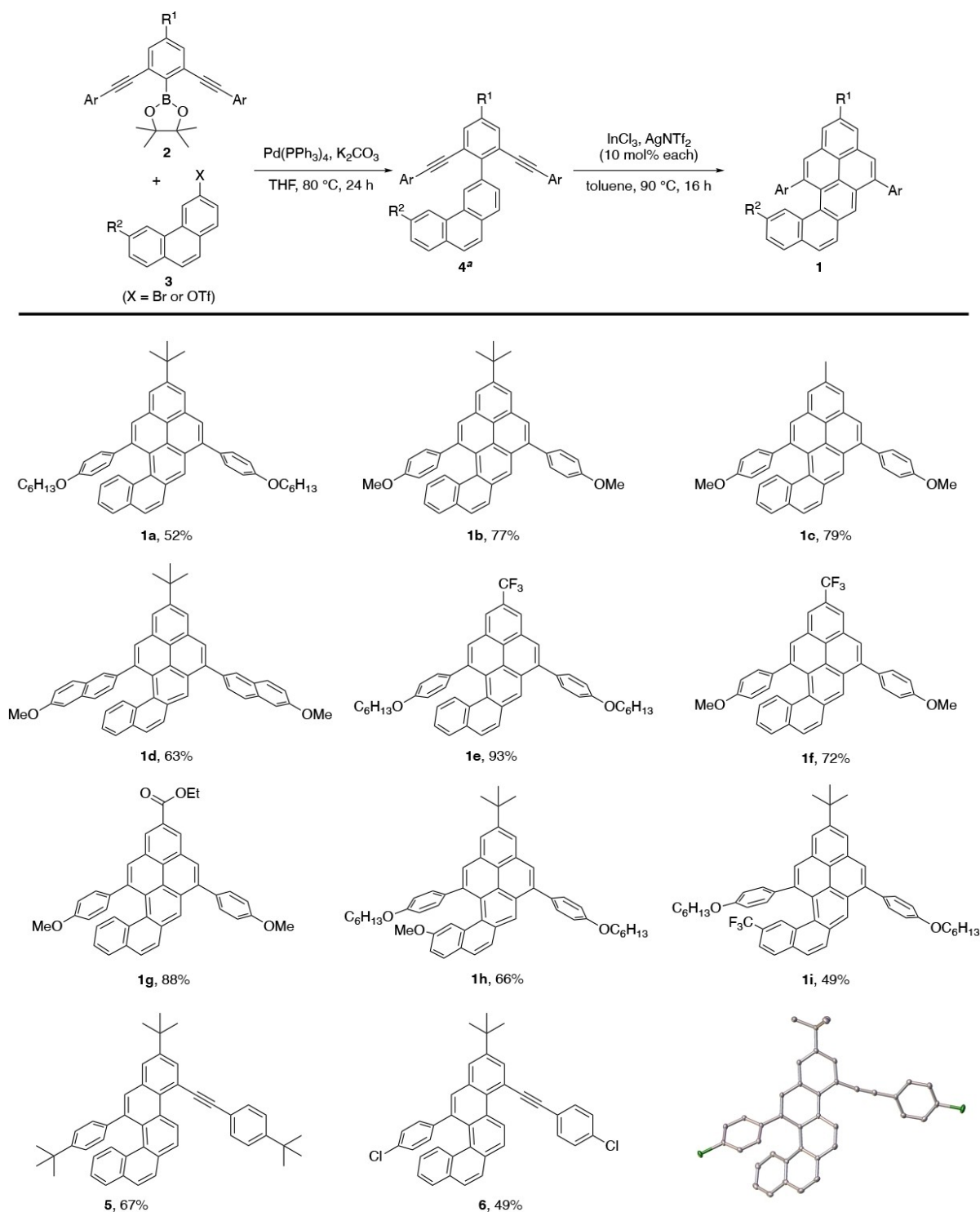Europe**
European Chemical
Societies Publishing

Figure 1. Synthesis of pyrene-helicene hybrids via (a) Brønsted acid catalyzed alkene-benzannulation,[5] (b) radical cascade three-point double annulation,[6] (c) photoredox chemistry,[7] (d) Brønsted acid-catalyzed four-fold alkyne benzannulations,[11] and (e) Lewis acid catalyzed two-fold alkyne benzannulations (this work).

the naphtho[1,2-a]pyrene products **1** (Scheme 1). The reaction works well with various electron-rich aryl (Ar) groups and R^1 as an alkyl group to improve solubility (**1a-d**). Electron withdrawing groups such as R^1=CF$_3$ (**1e** and **1f**) or an ester group (**1g**) resulted in good to excellent yields, respectively. Cyclization of both alkynes onto an electron-rich phenanthrene moiety (**4h**) worked well to give **1h** in good yield. The reaction on an electron-poor phenanthrene (**4i**) to give **1i** also worked, albeit with slightly lower yield. We found that reactions with less electron-rich aryl groups, such as Ar=4-tert-butylphenyl and 4-chlorophenyl, stalled at the monocyclization products **5** and **6**, respectively. Interestingly, the alkyne benzannulation reaction occurred regioselectively to give the helical benzo[c]chrysene products with the structure of compound **6** being unambiguously confirmed by X-ray crystallographic analysis (CCDC No. 2126201). Cyclization on the more sterically crowded side to produce a new cove region, as seen in **5** and **6**, has been observed in similar systems.[11] It should be noted that carrying out the reaction at higher temperatures only resulted in decomposition.

Chiral Separation

The conformation from the twisted π-system in compounds **1a–i**, **5**, and **6** renders these molecules chiral, and their M-P enantiomers are amenable to HPLC separation, provided the enantiomers are separated by a sufficiently high energy barrier. The M-P interconversion barriers of the complete set of naphtho[1,2-a]pyrenes **1b–i** and of the partially cyclized **5** (Scheme 1) were investigated. We used variable temperature dynamic high-performance liquid chromatography (DHPLC)[14] on a chiral stationary phase (CSP) for the determination of the enantiomerization barriers. Preliminary experiments showed that single enantiomers of **1b–i** and of **5** are prone to racemization at room temperature. However, excellent enantioseparations were achieved by lowering the column temperature between 0 °C and 10 °C, using a single enantioselective HPLC column packed with an immobilized amylose derivative CSP,[15] and a single mobile phase consisting of hexane/dichloromethane/methanol 90/10/1. Low-temperature HPLC separations of the enantiomers of **1h** and **1i** using ultraviolet and circular dichroism detections clearly demonstrate the enantiomeric relationship of the two species observed in each plot, showing equal intensity and opposite chiroptical signals (Figure 2).

When the HPLC column temperature was set to 0 °C, little or no on-column interconversion was detected for **1b–i** and **5**, as

EurJOC
European Journal of Organic Chemistry

Research Article
doi.org/10.1002/ejoc.202101466

Chemistry Europe
European Chemical
Societies Publishing

Scheme 1. Two-fold alkyne benzannulation reaction yielding naphtho[1,2-*a*]pyrenes **1a–i** and monocyclized benzo[c]chrysene products **5** and **6**. [a] Compound **4h** was synthesized using an alternate method. See Supporting Information for details.

judged from the absence of a plateau between the resolved peaks. At column temperatures between 10 °C and 20 °C, we observed temperature dependent deformations of the elution profiles and peak coalescence due to fast on-column *M-P* enantiomer interconversion for the majority of the examined compounds. For compounds **1h**, **1i** and **5**, the dynamic behavior was shifted to higher temperatures, with peak coalescence observed between 40 °C and 60 °C (see supporting information). We used computer simulation of the exchange broadened chromatograms to extract the apparent rate constants for the
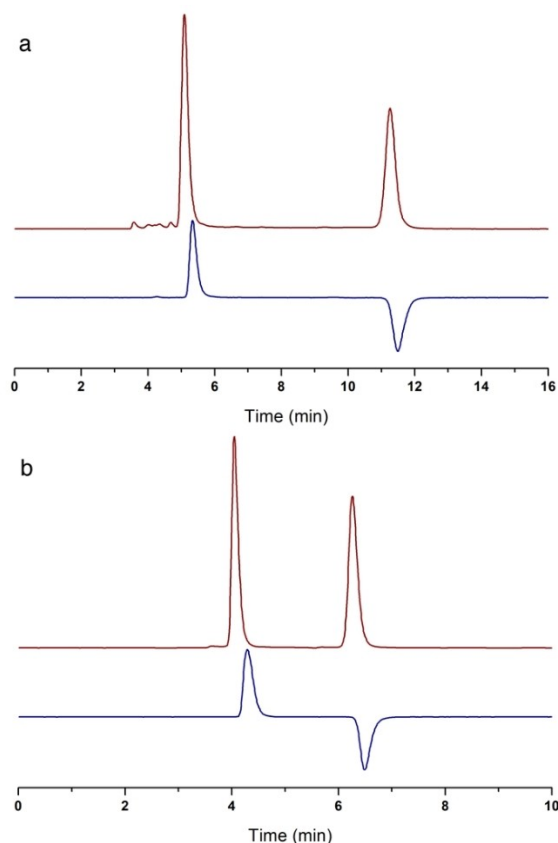
EurJOC
European Journal of Organic Chemistry

Research Article
doi.org/10.1002/ejoc.202101466

Chemistry
Europe
European Chemical
Societies Publishing

Figure 2. Enantioselective HPLC of **1h** (**a**) and **1i** (**b**) using UV (280 nm, red traces) and CD (300 nm, blue traces) detections.

on-column *M-P* interconversion process,[16] and from these values we calculated the corresponding free energy barriers of enantiomerization (Table 1).

The experimental Gibbs free energy of enantiomerization ($\Delta G^{\neq}$) for **1b–i** and **5** are gathered in Table 1, together with the retention factor of the first eluted enantiomer on the CSP. As expected, for the structurally similar **1b–i** naphtho[1,2-*a*]pyrene

Table 1. Rate constant and free energy barriers of enantiomerization.

Compound	k'_1[a] $T_{col} = 0\,°C$	$\Delta G^{\neq}$ (T)[b] [kcal/mol][c]	T[b] [°C]
1b	0.52	19.39	10
1c	1.06	19.53	10
1d	1.19	19.51	10
1e	0.26	19.61	10
1f	0.86	19.63	10
1g	1.92	19.72	10
1h	0.41	20.48	10
1i	0.13	21.36	20
5	0.05	20.04	10

[a] Retention factor of the 1st eluted enantiomer, defined as $(t_1-t_0)/t_0$ where t_1 is the elution time of the 1st eluted enantiomer and t_0 is the elution time of a non-retained compound. [b] Column temperature for the DHPLC experiments, T ±0.1 °C. [c] Gibbs free activation energy for the on-column enantiomerization (conversion of the 1st into the 2nd eluted enantiomer) at column temperature T, error ±0.02 kcal/mol.

series, enantiomerization barriers span a narrow range between 19.39 and 21.36 kcal/mol. The naphtho[1,2-*a*]pyrenes derived from unsubstituted phenanthrene ($R^2{<}C{=}{>}H$) show interconversion barriers between 19.39 and 19.72 kcal/mol, that correspond to half-life times between 20 and 30 s at 25 °C. Conversely, **1h** and **1i** (R^2 = methoxy and trifluoromethyl, respectively) have slightly higher interconversion energy barriers of 20.48 and 21.36 kcal/mol, respectively, and their *M-P* enantiomers have half-lives in the minutes range at 25 °C. This is likely due to the buttressing effect of the substituents in and near the *cove* region.[17] Clearly, *M-P* interconversion barriers in **1b–i** are mainly dependent on the presence of substituents at the terminal rings of the helix. Remote functionalization at the pyrene rings with methyl, *tert*-butyl, trifluoromethyl or ester groups has no effect on the interconversion barrier. The partially cyclized benzo[*c*]chrysene **5** shows a barrier equal to 20.04 kcal/mol, suggesting the stereochemical stability of the whole set of compounds is controlled by the number of *ortho*-condensed rings in the benzo[*c*]chrysene skeleton, by the size of the group on the terminal ring (R^2), and by the presence of a substituted aryl ring in the *cove* region.

CD spectra and configuration assignment of compounds **1h** and **1i**

Discrete amounts of the single enantiomers of **1h** and **1i** were obtained by low-temperature HPLC on a semipreparative column packed with the same CSP as the analytical separations. Wet fractions containing the individual enantiomers were used for the acquisition of their circular dichroism (CD) spectra. For these two compounds, comparison between experimental CD spectra and calculated ones is possible despite the low racemization barrier, as done for other [5]helicenes that racemize at room temperature.[18] Calculations have been performed considering the *P*-form of compounds **1h** and **1i**. Conformational analysis has been conducted considering just the most significant dihedral angles (Figure S10), assuming for simplicity that the aliphatic chains are transplanar and also substituting methoxy groups for hexyloxy chains. The orientation of the phenyl group in the *cove* region is dictated by steric hindrance due to the [4]helicene moiety (α1 dihedral angle, Figure S10), while the phenyl substituent on the opposite side shows two possible orientations. The hexyloxy/methoxy groups also exhibit two different orientations, giving a total of eight possible conformers for **1i** and sixteen for **1h** (due to the two possible conformers of methoxy group). Substitution of hexyloxy chains with methoxy groups seems to have a marginal influence on the conformer populations. The results of the conformational analysis of the compounds with methoxy groups is reported in Table S1 and Table S2 with the dihedral angles of only the significantly populated conformers reported. The reported values refer to IEFPCM calculations in hexane and are quite similar to the ones obtained in vacuo.

For all reported conformers, ECD spectra have been calculated. The phenyl and hexyloxy/methoxy orientations have some influence on the calculated ECD spectra, particularly considering

EurJOC
European Journal of Organic Chemistry

Research Article
doi.org/10.1002/ejoc.202101466

Chemistry
Europe
European Chemical
Societies Publishing

the higher energy bands. Calculations for all conformers for the solvated case are reported in Figure S1 and Figure S2. Similar effects of substituents on the high energy bands had already been observed in other helicene hybrids despite the quite extended and distorted π-system.[11] Substitution of hexyloxy with methoxy seems to play a minor role on the calculated ECD spectra. The final results for the two molecules are reported in Figure 3 after applying a wavelength red-shift as indicated in the caption, analogous to the one used with a similar level of calculations. The correspondence with the experimental spectra of the first eluted fraction is quite good for the two compounds, permitting a safe assignment of the configuration, namely the *P* form for the two molecules. We notice that the succession of band signs is correctly predicted; the lowest energy bands are well reproduced and are the ones also showing low sensitivity to conformational changes. We find that the wavelength difference among the observed features is better reproduced by the calculations based on the presence of solvent (we considered hexane for simplicity). The low sensitivity of the lowest energy CD band to the pendant conformation is strictly connected to the laterally extended π-system in comparison with carbohelicene. In this last case, it is well known that the lowest energy bands correspond to forbidden transitions,[19] a fact that limits their use for optoelectronic applications as opposed to the cases with helicene or helicenoid compounds with heteroatoms.[20] In the two compounds herein considered, the extended carbon-atom backbone gives rise to dipole and rotational strength of the lowest energy transition, which are non-negligible due to the pyrene moiety. From the calculations, we conclude that the electric dipole moment of the lowest energy transition (HOMO-LUMO) is nearly parallel to the pyrene long axis, while the

magnetic dipole transition moment forms an angle of about 80°, pointing out of the pyrene plane, which is enough to give good rotational strength. In Figure S13, one may consider the HOMO and LUMO orbitals for the most populated conformer of the two molecules **1h** and **1i**, which are localized on the pyrene-helicene backbone, justifying their sensitivity to configuration.

IR and Raman spectroscopy

The analysis of the IR spectra of **1b–i**, fostered by DFT calculations, reveals several characteristic signals associated to the different functional groups attached to the helical nano-graphene core (Figure 4). Here we highlight just a few notable spectroscopic features, identified in Figure 4 by boxes; the complete assignments are discussed in the Supporting Information. In the low wavenumber region (box 14), we find a series of signals assigned to collective out-of-plane CH bending: the compounds **1c**, **1b**, **1g**, **1f**, **1e** share the same CH bond topology at the edge of the helical nanographene core, which reflects in the remarkably similar spectral pattern of this region. The trifluoromethyl functionalization of compounds **1e**, **1f**, and **1i** is evidenced by the similar spectral features in the box 11 region. Remarkably, the different location of the functionalization found in **1i** (R²) *vs* **1e** and **1f** (R¹) is evidenced by the shift of the CF₃ signals from box 6 to box 7, respectively.[21] Finally, the functionalization by the methoxy group in compounds **1c**, **1b**, **1g**, **1f**, and **1d** is confirmed by the characteristic peak identified by boxes 12 and 13.

Interestingly, as documented by the tables found in Supporting Information, it is not possible to find a single IR marker of the
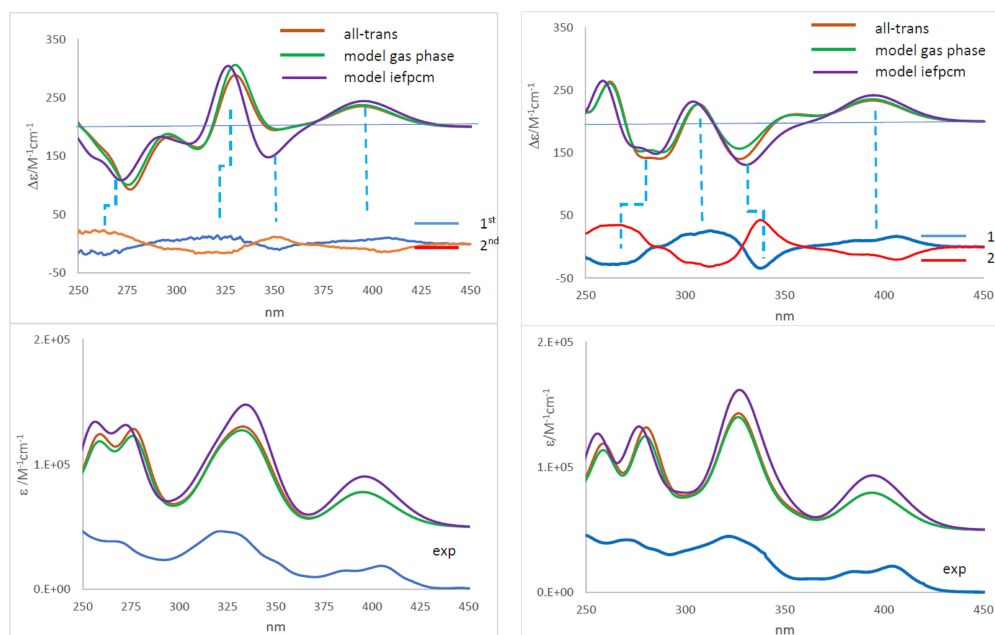

Figure 3. Comparison of calculated and experimental ECD and absorption spectra of compounds **1h** (left) and **1i** (right), recorded at 10^{-5} M concentration. Calculations have been performed considering all transplanar aliphatic chains and methoxy substitution (model compounds) in the gas phase and at the IEFPCM level, in all cases a Boltzmann weighted average has been performed. Red-shift has been applied to calculated spectra by 40 nm for the gas phase and by 35 nm when implicit solvent model has been considered.
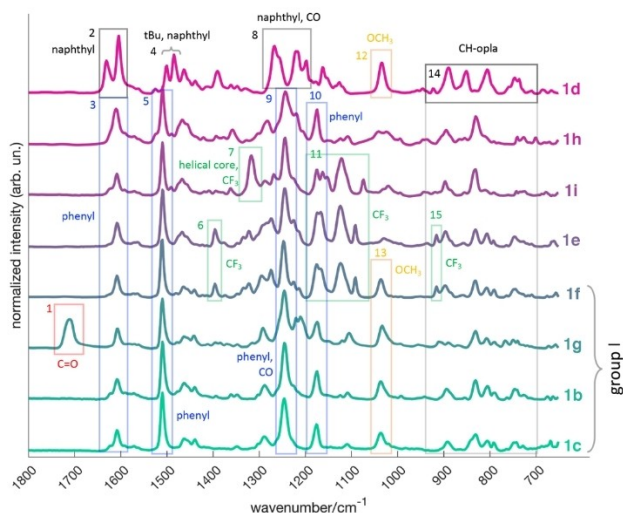
EurJOC
European Journal of Organic Chemistry

Research Article
doi.org/10.1002/ejoc.202101466

Chemistry
Europe
European Chemical
Societies Publishing

Figure 4. The experimental micro FT-IR spectra of compounds **1 b–i** across the fingerprint region. The contributions from specific functional groups are highlighted with numbered boxes (see text).

nanographene core. The vibrations of this part of the molecule are always coupled with vibrations of the functional groups. Essentially, only the CH out-of-plane wavenumber region can be considered, as a whole, a fingerprint of the nanographene shape.

With Raman spectroscopy, the situation is quite different. The comparison of Figure 5 with Figure 4 highlights the complementarity of IR and Raman: the expected G and D bands of such nanographenes are markers of the structure of the extended π-conjugated core. We do not observe obvious Raman markers of the functional groups, with the only exception of the weak CO stretching feature observed for compound **1g** (slightly above 1700 cm^{-1}, Figure 5). However, the pattern of the G band and
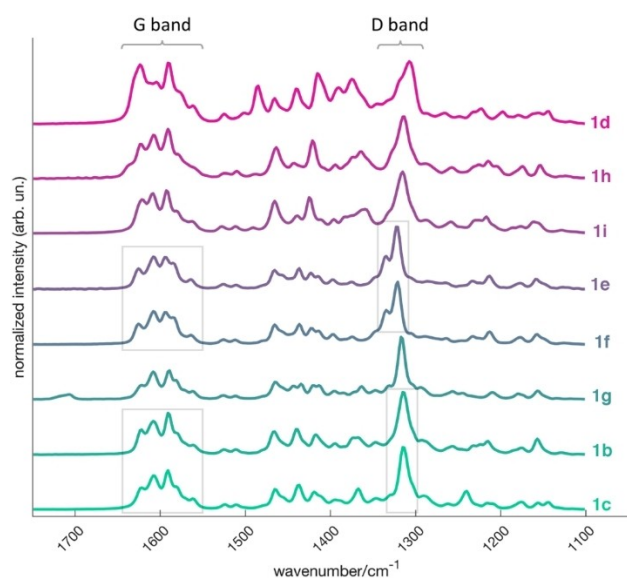
the position of the D peak are remarkably sensitive to the functional groups attached to the nanographene core. Compounds **1b** and **1c** essentially share the same substituents [the difference between a *tert*-butyl (**1b**) and methyl (**1c**) substituent is not much from the point of view of the effect on π-conjugation]. By consequence, the position of the D peak in the two compounds is essentially the same (1314 cm^{-1}) as is the pattern of the G band. Compared with **1b** and **1c**, the ethyl-ester substituent of **1g** very slightly changes the pattern of the G band and the position of the D peak (1317 cm^{-1}). Compounds **1e** and **1f** share the trifluoromethyl functionalization at R^1, and the 4-methoxyphenyl/4-hexyloxyphenyl functionalization (Ar) has the same influence on π-conjugation. Therefore, as expected, **1e** and **1f** exhibit the same G band pattern and the same position of the D peak (1321 cm^{-1}). The Raman spectra of **1h** and **1i** are rather close, from which we infer that the inductive effect caused by the methoxy and trifluoromethyl R^2 substituents on the nanographene core are rather close. This observation is consistent with the similarity of the position of the π-π* electronic transitions of **1h** and **1i** (see CD spectroscopy section). Finally, the G and D band of compound **1d** appear significantly different from the previous compounds given the sizeable contributions from the π-conjugated naphthyl substituents to the Raman spectrum.

Conclusion

In summary, we have developed a successful and efficient synthesis of functionalized naphtho[1,2-*a*]pyrenes by utilizing a two-fold alkyne benzannulation reaction. The reaction is catalyzed by a mixture of indium chloride and silver bistriflimide to afford the products in moderate to excellent yields. The separation of enantiomers can be done at low temperatures and analysis of the enantiomerization process shows a higher barrier than regular [4]helicenes. This is due to steric repulsion in the *cove* region due to substitution. Adding substituents to the backbone of the nanographene, near the *cove* region, further increases the inversion barrier of these molecules and could serve as a design element to arrive at persistently chiral [4]helicene-like nanographenes. The lifetime of the enantiopure substrates is long enough to allow for analysis by CD spectroscopy. The ECD spectra were consistent with calculated values, which assisted in the assignment of absolute stereochemistry. Functionality around the nanographene core is discernable by IR spectroscopy while Raman spectroscopy serves as a great complimentary tool for looking at the extended π-conjugated backbone structure. Further studies on extending this methodology to the synthesis of larger π-extended helicene-like structures is ongoing in our lab.

Experimental Section

Crystallographic data: Deposition number 2126201 (for **6**) contains the supplementary crystallographic data for this paper. These data are provided free of charge by the joint Cambridge Crystallographic

Figure 5. The experimental micro FT-Raman spectra of compounds **1 b–i** across the G and D-band regions. The grey boxes identify similar patterns and positions of the G and D bands (see text).

EurJOC
European Journal of Organic Chemistry

Research Article

doi.org/10.1002/ejoc.202101466

Chemistry Europe
European Chemical Societies Publishing

Data Centre and Fachinformationszentrum Karlsruhe Access Structures service www.ccdc.cam.ac.uk/structures.

Conflict of Interest

The authors declare no conflict of interest.

Data Availability Statement

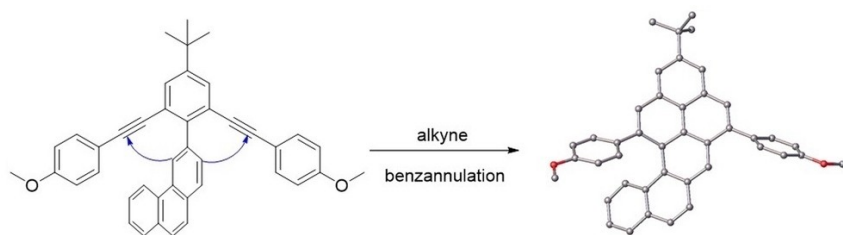The data that support the findings of this study are available in the supplementary material of this article.

[1] a) A. Narita, X.-Y. Wang, X. Feng, K. Müllen, *Chem. Soc. Rev.* **2015**, *44*, 6616–6643; b) K. M. Magiera, V. Aryal, W. A. Chalifoux, *Org. Biomol. Chem.* **2020**, *18*, 2372–2386; c) A. D. Senese, W. A. Chalifoux, *Molecules* **2018**, *24*, 118; d) E. M. Muzammil, D. Halilovic, M. C. Stuparu, *Commun. Chem.* **2019**, *2*, 58.

[2] a) J. Wu, W. Pisula, K. Müllen, *Chem. Rev.* **2007**, *107*, 718–747; b) J. Mei, Y. Diao, A. L. Appleton, L. Fang, Z. Bao, *J. Am. Chem. Soc.* **2013**, *135*, 6724–6747; c) S. Sergeyev, W. Pisula, Y. H. Geerts, *Chem. Soc. Rev.* **2007**, *36*, 1902–1929; d) M. Ball, Y. Zhong, Y. Wu, C. Schenck, F. Ng, M. Steigerwald, S. Xiao, C. Nuckolls, *Acc. Chem. Res.* **2015**, *48*, 267–276.

[3] a) Y. Shen, C.-F. Chen, *Chem. Rev.* **2012**, *112*, 1463–1535; b) M. Gingras, *Chem. Soc. Rev.* **2013**, *42*, 968–1006; c) M. Gingras, G. Félix, R. Peresutti, *Chem. Soc. Rev.* **2013**, *42*, 1007–1050; d) M. Gingras, *Chem. Soc. Rev.* **2013**, *42*, 1051–1095.

[4] a) Y. Hu, G. M. Paternò, X.-Y. Wang, X.-C. Wang, M. Guizzardi, Q. Chen, D. Schollmeyer, X.-Y. Cao, G. Cerullo, F. Scotognella, K. Müllen, A. Narita, *J. Am. Chem. Soc.* **2019**, *141*, 12797–12803; b) M. Buchta, J. Rybáček, A. Jančařík, A. A. Kudale, M. Buděšínský, J. V. Chocholoušová, J. Vacek, L. Bednárová, I. Císařová, G. J. Bodwell, I. Starý, I. G. Stará, *Chem. Eur. J.* **2015**, *21*, 8910–8917; c) A. k Swain, K. Kolanji, C. Stapper, P. Ravat, *Org. Lett.* **2021**, *23*, 1339–1343.

[5] a) D. Desai, A. K. Sharma, J.-M. Lin, J. Krzeminski, M. Pimentel, K. El-Bayoumy, S. Nesnow, S. Amin, *Chem. Res. Toxicol.* **2002**, *15*, 964–971; b) A. K. Sharma, J. Krzeminski, D. Desai, S. Amin, *Polycyclic Aromat. Compd.* **2003**, *23*, 297–305.

[6] R. K. Kawade, C. Hu, N. R. Dos Santos, N. Watson, X. Lin, K. Hanson, I. Alabugin, *Angew. Chem. Int. Ed.* **2020**, *59*, 14352–14357; *Angew. Chem.* **2020**, *132*, 14458–14463.

[7] A.-C. Bédard, A. Vlassova, A. C. Hernandez-Perez, A. Bessette, G. S. Hanan, M. A. Heuft, S. K. Collins, *Chem. Eur. J.* **2013**, *19*, 16295–16302.

[8] a) W. Yang, R. Bam, V. J. Catalano, W. A. Chalifoux, *Angew. Chem. Int. Ed.* **2018**, *57*, 14773–14777; *Angew. Chem.* **2018**, *130*, 14989–14993; b) W. Yang, W. A. Chalifoux, *Synlett* **2017**, *28*, 625–632; c) W. Yang, R. R. Kazemi, N. Karunathilake, V. J. Catalano, M. A. Alpuche-Aviles, W. A. Chalifoux, *Org. Chem. Front.* **2018**, *5*, 2288–2295; d) W. Yang, J. H. S. K. Monteiro, A. de Bettencourt-Dias, V. J. Catalano, W. A. Chalifoux, *Angew. Chem. Int. Ed.* **2016**, *55*, 10427–10430; *Angew. Chem.* **2016**, *128*, 10583–10586; e) W. Yang, J. H. S. K. Monteiro, A. de Bettencourt-Dias, V. J. Catalano, W. A. Chalifoux, *Chem. Eur. J.* **2019**, *25*, 1441–1445; f) W. Yang, J. H. S. K. Monteiro, A. de Bettencourt-Dias, W. A. Chalifoux, *Can. J. Chem.* **2016**, *95*, 341–345.

[9] W. Yang, G. Longhi, S. Abbate, A. Lucotti, M. Tommasini, C. Villani, V. J. Catalano, A. O. Lykhin, S. A. Varganov, W. A. Chalifoux, *J. Am. Chem. Soc.* **2017**, *139*, 13102–13109.

[10] W. Yang, A. Lucotti, M. Tommasini, W. A. Chalifoux, *J. Am. Chem. Soc.* **2016**, *138*, 9137–9144.

[11] R. Bam, W. Yang, G. Longhi, S. Abbate, A. Lucotti, M. Tommasini, R. Franzini, C. Villani, V. J. Catalano, M. M. Olmstead, W. A. Chalifoux, *Org. Lett.* **2019**, *21*, 8652–8656.

[12] P. Sitaula, R. J. Malone, G. Longhi, S. Abbate, E. Gualtieri, A. Lucotti, M. Tommasini, R. Franzini, C. Villani, V. J. Catalano, W. A. Chalifoux, *ChemRxiv.* Cambridge: Cambridge Open Engage; **2020**; This content is a preprint and has not been peer-reviewed. DOI: 10.26434/chemrxiv.12931703.v1.

[13] a) F. B. Mallory, C. W. Mallory, *J. Org. Chem.* **1983**, *48*, 526–532; b) H. R. Talele, M. J. Gohil, A. V. Bedekar, *Bull. Chem. Soc. Jpn.* **2009**, *82*, 1182–1186.

[14] a) D. Casarini, L. Lunazzi, S. Alcaro, F. Gasparrini, C. Villani, *J. Org. Chem.* **1995**, *60*, 5515–5519; b) C. Villani, W. H. Pirkle, *Tetrahedron: Asymmetry* **1995**, *6*, 27–30; c) I. D'Acquarica, F. Gasparrini, M. Pierini, C. Villani, G. Zappia, *J. Sep. Sci.* **2006**, *29*, 1508–1516; d) O. Trapp, V. Schurig, *J. Am. Chem. Soc.* **2000**, *122*, 1424–1430; e) F. Maier, O. Trapp, *Angew. Chem. Int. Ed. Engl.* **2012**, *51*, 2985–2988; f) S. Mortera Levi, R. Sabia, M. Pierini, F. Gasparrini, C. Villani, *Chem. Commun.* **2012**, *48*, 3167–3169; g) O. Trapp, *Top. Curr. Chem.* **2013**, *341*, 231–269; h) R. Sabia, A. Ciogli, M. Pierini, F. Gasparrini, C. Villani, *J. Chromatogr. A* **2014**, *1362*, 144–149; i) C. Viglianisi, C. Biagioli, M. Lippi, M. Pedicini, C. Villani, R. Franzini, S. Menichetti, *Eur. J. Org. Chem.* **2019**, *2019*, 164–167.

[15] T. Zhang, C. Kientzy, P. Franco, A. Ohnishi, Y. Kagamihara, H. Kurosawa, *J. Chromatogr. A* **2005**, *1075*, 65–75.

[16] a) V. Schurig, *Chirality* **2005**, *17*, S205–S226; b) C. Wolf, *Chem. Soc. Rev.* **2005**, *34*, 595–608; c) O. Trapp, *Anal. Chem.* **2006**, *78*, 189–198; d) O. Trapp, *J. Chromatogr. B* **2008**, *875*, 42–47; e) R. Cirilli, R. Costi, R. Di Santo, F. La Torre, M. Pierini, G. Siani, *Anal. Chem.* **2009**, *81*, 3560–3570.

[17] a) P. Ravat, *Chem. Eur. J.* **2021**, *27*, 3957–3967; b) R. N. Armstrong, H. L. Ammon, J. N. Darnow, *J. Am. Chem. Soc.* **1987**, *109*, 2077–2082.

[18] a) F. Lebon, G. Longhi, F. Gangemi, S. Abbate, J. Priess, M. Juza, C. Bazzini, T. Caronna, A. Mele, *J. Phys. Chem. A* **2004**, *108*, 11752–11761; b) S. Abbate, C. Bazzini, T. Caronna, F. Fontana, F. Gangemi, F. Lebon, G. Longhi, A. Mele, I. Natali Sora, *Inorg. Chim. Acta* **2007**, *360*, 908–912.

[19] a) O. E. Weigang Jr, J. A. Turner, P. A. Trouard, *J. Chem. Phys.* **1966**, *45*, 1126–1134; b) Y. Nakai, T. Mori, Y. Inoue, *J. Phys. Chem. A* **2012**, *116*, 7372–7385; c) S. Abbate, G. Longhi, F. Lebon, E. Castiglioni, S. Superchi, L. Pisani, F. Fontana, F. Torricelli, T. Caronna, C. Villani, R. Sabia, M. Tommasini, A. Lucotti, D. Mendola, A. Mele, D. A. Lightner, *J. Phys. Chem. C* **2014**, *118*, 1682–1695; d) Y. Liu, J. Cerezo, G. Mazzeo, N. Lin, X. Zhao, G. Longhi, S. Abbate, F. Santoro, *J. Chem. Theory Comput.* **2016**, *12*, 2799–2819.

[20] K. Dhbaibi, L. Favereau, J. Crassous, *Chem. Rev.* **2019**, *119*, 8846–8953.

[21] S. Abbate, G. Longhi, G. Mazzeo, C. Villani, S. Petković, R. Ruzziconi, *RSC Adv.* **2019**, *9*, 11781–11796.

RESEARCH ARTICLE

A mild Lewis acid-catalyzed double alkyne benzannulation reaction onto a phenathrene moiety results in the rapid synthesis of π-extended [4]helicene hybrids. Substitution of the cove region results in increased inversion barriers and allows for separation and study of the enantiomers by circular dichroism.

Prof. W. A. Chalifoux*, Dr. P. Sitaula, R. J. Malone, Dr. G. Longhi, Prof. S. Abbate, E. Gualtieri, Dr. A. Lucotti, Prof. M. Tommasini, R. Franzini, Prof. C. Villani, Prof. V. J. Catalano

1 – 8

π-Extended Helical Nanographenes: Synthesis and Photophysical Properties of Naphtho[1,2-a]pyrenes